analytical chemistry

Letter

Cite This: Anal. Chem. 2018, 90, 7127−7130

pubs.acs.org/ac

Potential-Controlled Adsorption, Separation, and Detection of Redox Species in Nanofluidic Devices

Jin Cui, Klaus Mathwig,[†] Dileep Mampallil,[‡] and Serge G. Lemay*

MESA+ Institute for Nanotechnology, University of Twente, PO Box 217, 7500 AE Enschede, The Netherlands

Supporting Information

ABSTRACT: Nanoscale channels and electrodes for electrochemical measurements exhibit extreme surface-to-volume ratios and a correspondingly high sensitivity to even weak degrees of surface interactions. Here, we exploit the potential-dependent reversible adsorption of outer-sphere redox species to modulate in space and time their concentration in a nanochannel under advective flow conditions. Induced concentration variations propagate downstream at a species-dependent velocity. This allows one to amperometrically distinguish between attomole amounts of species based on their time-of-flight. On-demand concentration pulse generation, separation, and detection are all integrated in a miniaturized platform.

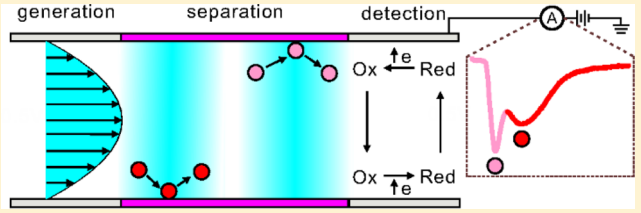

There is widespread interest in methods capable of performing complex analysis on ultrasmall sample volumes such as those encountered in single-cell analysis.[1,2] This level of miniaturization however requires a reimagining of traditional analytical approaches. A prime example is liquid chromatography in nanoscale fluidic "columns".[3−7] Because of the extremely high surface-to-volume ratios prevailing here, the traditional stationary phase can be complemented or even substituted by interactions with the walls of the channel. Downscaling detection methods poses similar challenges. Electrochemical methods are particularly well suited since electrodes are readily miniaturized and mass transport scales favorably with electrode size.[8] Electrochemistry has been widely applied as detection modality in high-performance liquid chromatography (HPLC) for at least three decades and is particularly important for detecting nonfluorescent species.[9−12] However, while separation eases the burden of detection downstream, electrochemical methods remain susceptible to interfering species. A wide array of surface based approaches has been developed to mitigate interference,[13−30] which becomes even more efficient in miniaturized systems with higher surface-to-volume ratios.

Here, we combine these elements and demonstrate how surface interactions in nanoscale channels can be used to electrochemically generate, separate, and detect analyte pulses on demand in a compact integrated device. This approach, illustrated in Figure 1, allows one to discriminate between nonfluorescent species in samples with subpicoliter volumes using conventional electrochemical instrumentation. The actual device, shown in Figure 1a, consists of a silicon oxide nanochannel (height of 330 nm, width of 5 μm) in parallel with a polydimethylsiloxane microchannel (PDMS, height of 3 μm, width of 5 μm). This parallel-flow configuration allows one to create a convective flow along the nanochannel.[31,32] The average flow speed in the nanochannel is controlled by a syringe pump and is estimated at 24 μm/s flow speed per μL/h pump rate based on the Hagen−Poiseuille law.[33] Two nanogap transducers are located 500 μm apart along the channel, each consisting of a pair of electrodes embedded in the floor and ceiling of the nanochannel (lengths of 102 and 108 μm for the top and bottom electrodes, respectively). Devices fabrication is described in the Supporting Information.

In a typical experiment, aqueous solutions of 50 μM 1,1′-ferrocenedimethanol ($Fc(MeOH)_2$), (feccocenylmethyl)-trimethylammonium ($FcTMA^+$), or ferrocyanide ($[Fe(CN)_6]^{4-}$) and 1 M KCl were pumped at a constant rate through the nanochannel. The potentials of the downstream top and bottom electrodes were held at 0.5 and 0 V, respectively, versus an Ag/AgCl reference electrode located downstream. This corresponds to large oxidizing and reducing overpotentials, respectively, for all three species investigated. Thus, while these species have different formal potentials, we do not exploit this fact to discriminate between them. Instead, redox cycling takes place between the two electrodes for all three species with a diffusion-limited redox-cycling current given by $I_{rc}(t) = nFADc(t)/z$, where n is the number of electrons transferred per cycle, F is the Faraday constant, A (= 300 μm^2) is the overlap area between the two electrodes, z (= 330 nm) is the electrode spacing, D is the diffusion coefficient of the redox species, and $c(t)$ is the time-dependent average concentration of the redox species in the detection volume. This expression also holds under flow conditions because the transverse diffusion time (~80 μs) is much shorter than the transit time through the detection volume (~0.14 s at the fastest flow rates, corresponding to a Graetz number (Gz) ≈ 6 × 10^{-4}).[32] This also ensures that practically all molecules transported through the upstream nanogap equilibrate with its

Received: April 17, 2018
Accepted: May 24, 2018
Published: May 29, 2018

DOI: 10.1021/acs.analchem.8b01719
Anal. Chem. 2018, 90, 7127−7130

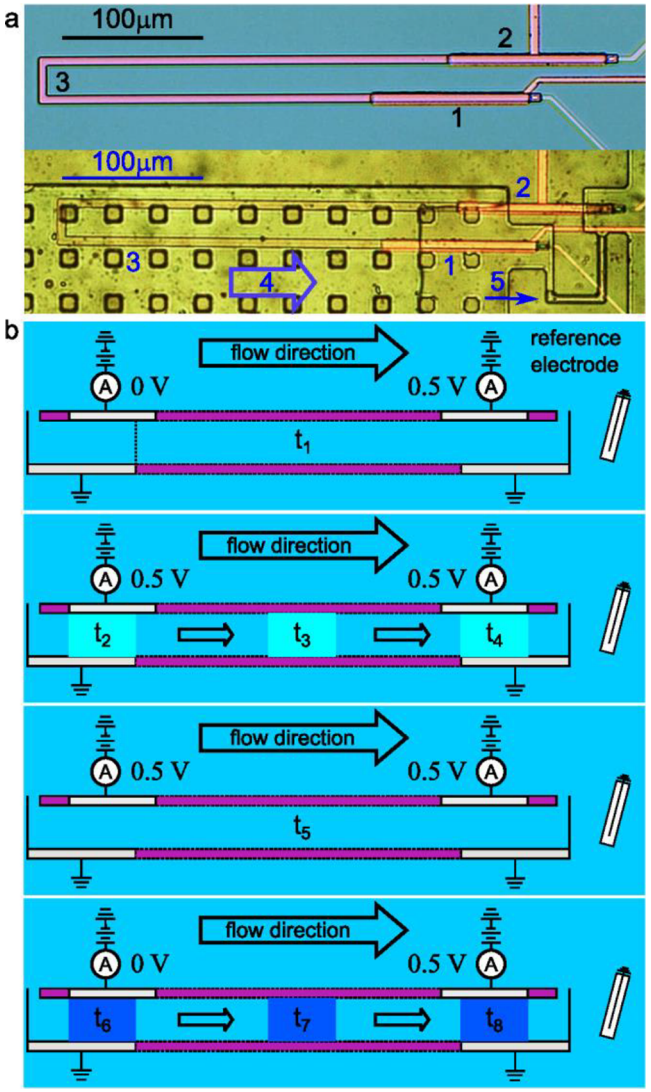

Figure 1. (a) Device before etching of the nanochannel (top) and etched device interfaced to a PDMS microchannel (bottom; the image appears grainy as it was captured through ~4 mm PDMS). The device consists of two nanogap transducers (1 and 2), a nanochannel used for separation (3), a microfluidic inlet (4, arrow shows flow direction), and a microchannel (5) in parallel with the nanochannel. (b) Working principle, as described in the text.

top electrode since it extends 2 μm further downstream, as sketched in Figure 1b.

The degree of adsorption to an electrode depends on the interfacial potential.[8,34−36] We exploit this effect to locally modulate the concentration of redox-active analytes in the channel. As illustrated in Figure 1b, the potential of the upstream top electrode is initialized at 0 V (time t_1) and then switched to 0.5 V at t_2. This causes the analyte to adsorb further to the electrodes, creating a plug with depleted concentration in the channel. This plug is advected along the nanochannel (t_3), resulting in a temporary decrease of the redox-cycling current (I_{rc}) when it reaches the downstream nanogap (t_4). As the flow brings fresh analyte into the nanochannel, both upstream and downstream transducers return to the steady state (t_5). The opposite process occurs when the upstream potential is switched back to 0 V (t_6 to t_8).

Figure 2 shows typical results for all three redox species. Figure 2a,b shows the signals at the upstream and downstream

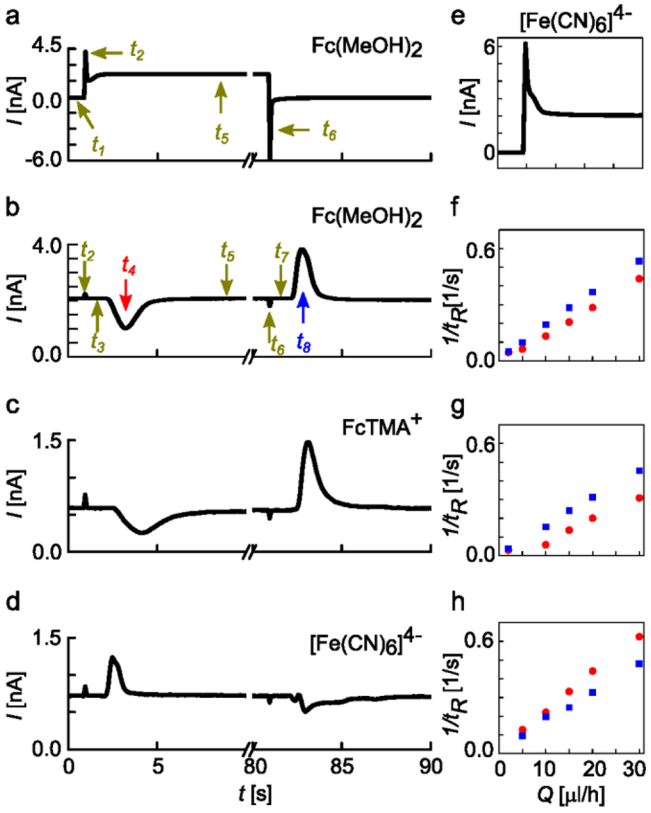

Figure 2. Redox cycling currents in the (a) upstream and (b) downstream transducers for $Fc(MeOH)_2$ upon applying a square wave potential to one of the upstream electrodes. The labels t_1 to t_8 refer to the sketches in Figure 1b. (c, d) Downstream responses for $FcTMA^+$ and $[Fe(CN)_6]^{4-}$, respectively. (e) Upstream response observed simultaneously with (d). (a−e) Measured at a pump rate of 30 μL/h. (f−h) Inverse retention time of oxidized (red) and reduced (blue) forms versus pump rate for $Fc(MeOH)_2$, $FcTMA^+$, and $[Fe(CN)_6]^{4-}$, respectively.

top electrodes, respectively, for $Fc(MeOH)_2$. Upon applying a potential step at t_2, redox cycling is initiated at the upstream transducer and a sharp cross-talk spike is observed in the downstream one. The upstream current does not directly jump to its steady state level, however; instead, it increases gradually while the adsorption-depleted plug at this electrode is replaced by fresh solution.[35] The 0.6 nA magnitude of the initial dip in the current corresponds to only 1.0 attomole $Fc(MeOH)_2^+$ adsorbing to the electrode upon stepping the voltage, illustrating the absolute sensitivity of the nanogap transducer. Several seconds later, a corresponding decrease in redox-cycling current is observed at the downstream transducer as the leading edge of the depleted region reaches its position. Surprisingly, however, the magnitude of this decrease, 1.06 nA, corresponds to a depletion of 1.8 attomole, which is larger than that observed at the upstream electrode. This indicates that additional molecules, now in their oxidized form, were lost in transit via adsorption to the SiO_2 channel walls.[37,38] With continued flow, the surfaces eventually come to equilibrium with the solution again and I_{rc} returns to its steady state value. The reverse process occurs at time t_6, when the upstream electrode potential is stepped downward and molecules are released from its surface.

Similar behavior is observed with $FcTMA^+$, as shown in Figure 2c. The opposite behavior is however observed for

DOI: 10.1021/acs.analchem.8b01719
Anal. Chem. 2018, 90, 7127−7130

$[Fe(CN)_6]^{4-}$ (Figure 2d). Here, stepping the top electrode to 0.5 V results in a temporary concentration increase at the top transducer (Figure 2e), followed by a subsequent increase in current at the downstream detector. This indicates decreased adsorption of ferricyanide at 0.5 V compared to ferrocyanide at 0 V.

Figure 2f–h shows the inverse of the retention time, $1/t_R$, versus the pump flow rate. Here, t_R is the time at which the peak current is observed (t_4, t_8) with respect to the switching time of the upstream electrode (t_2, t_6); $1/t_R$ is approximately proportional to the propagation speed and varies linearly with pump rate, as expected.

Interestingly, Figure 2 shows that the transit times are different for the three species. They are also influenced by the potential of the upstream top electrode, which sets the redox state of the molecules being transported downstream. This provides further evidence that the redox molecules undergo reversible adsorption to the SiO_2 channel walls which slows down their transport.[33,38]

Species-dependent transit times suggest the feasibility of separating species in nanochannels. Figure 3 shows results for a 1:1 mixture of $Fc(MeOH)_2$ and $FcTMA^+$ at different flow rates. The amperometric response in this case exhibits two peaks, each presumably corresponding to a single species. Measurements with different ratios of the two analytes (Supporting Information) confirms the assignment of the first and second peaks to $Fc(MeOH)_2$ and $FcTMA^+$, respectively, consistent with the peak time data of Figure 2f,g. The differences in capacity (retention) factors between the individual species and the mixture are discussed further in the Supporting Information. In summary, competition between the species for adsorption sites leads to a relative enhancement of $FcTMA^+$ adsorption and a corresponding suppression for $Fc(MeOH)_2$ compared to the pure species at the same total concentration. Conceptually, the ratio of retention factors for species i in the mixed and monocomponent system can be expressed as $k'_{i,mixt}/k'_{i,mono} = ((1 + a^{(-1)^{i-1}})/2)^{n_i-1}$, where $i = 1$ and 2, n_i is a constant for each species i, and a is the so-called dimensionless competition coefficient. Our observations are consistent with the case $a \neq 1$. Combinations of $[Fe(CN)_6]^{4-}$ with the other two species did not yield a clear peak signal, on the other hand, presumably because its opposite response to potential changes leads to partial cancellation of the signals.

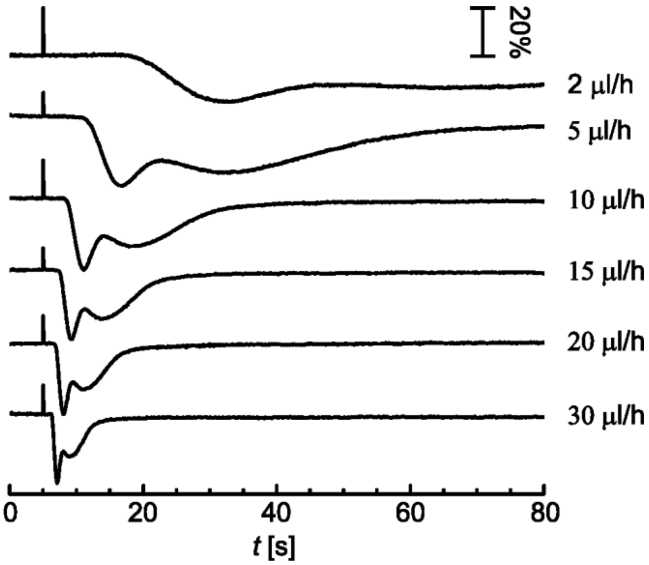

Figure 3. Normalized redox cycling currents for a 1:1 mixture of $Fc(MeOH)_2$ and $FcTMA^+$ at different pump rates. The scale bar represents a variation of the current of 20% compared to its baseline value. The traces have been offset vertically for clarity.

These experiments demonstrate directly the occurrence of potential-dependent, reversible adsorption of outer sphere redox species. This can be utilized to create localized concentration perturbations, enabling a form of electrochemical chromatography. On the basis of continuous sample flow and "on-demand" sample plug generation, attomole analyte quantities were separated in short 20 s retention times. Similar behavior can be expected in other nanoscale geometries and in porous materials with comparably high surface-to-volume ratios.

It has been demonstrated that chromatography in nanochannels can achieve high retention factors.[3,7] The device employed here, however, did not maximize discriminating power, which can be significantly improved through geometry optimization (e.g., shorter control electrodes and longer separation channel; see Supporting Information) and tuning of the adsorption properties of the channel. This may be achieved in a controlled and tunable manner by placing an additional "gate" electrode along the channel whose potential could be tuned to optimize separation.[39,40] Finally, we note that the device described can be realized in a variety of geometries including a needle-shaped microprobe suitable for in vivo studies.

■ ASSOCIATED CONTENT

Supporting Information

The Supporting Information is available free of charge on the ACS Publications website at DOI: 10.1021/acs.analchem.8b01719.

Fabrication of the nanofluidic devices (Figure S-1), amperometric data for different ratio mixtures (Figure S-2), capacity (or retention) factor (Figure S-3) and their interpretation (Figure S-4), multicomponent Freundlich isotherm model calculation, and optimization of geometry (Figure S-5) (PDF)

■ AUTHOR INFORMATION

Corresponding Author

*E-mail: s.g.lemay@utwente.nl. Tel: +31(0)534892306.

ORCID

Jin Cui: 0000-0001-9659-4381

Klaus Mathwig: 0000-0002-8532-8173

Present Addresses

†K.M.: University of Groningen, Groningen Research Institute of Pharmacy, Pharmaceutical Analysis, P.O. Box 196, 9700 AD Groningen, The Netherlands.

‡D.M.: Indian Institute of Science Education & Research Tirupati, Mangalam P.O., Tirupati 517507, India.

Author Contributions

The manuscript was written through contributions of all authors. All authors have given approval to the final version of the manuscript.

Notes

The authors declare no competing financial interest.

DOI: 10.1021/acs.analchem.8b01719
Anal. Chem. 2018, 90, 7127–7130

■ ACKNOWLEDGMENTS

The authors gratefully acknowledge fruitful conversations with J.C.T. Eijkel and J. Quist. Financial support was provided by The Netherlands Organization for Scientific Research (NWO) and the European Research Council (ERC) under project number 278801.

■ REFERENCES

(1) Mazutis, L.; Gilbert, J.; Ung, W. L.; Weitz, D. A.; Griffiths, A. D.; Heyman, J. A. *Nat. Protoc.* **2013**, *8* (5), 870−891.
(2) Mawatari, K.; Kazoe, Y.; Shimizu, H.; Pihosh, Y.; Kitamori, T. *Anal. Chem.* **2014**, *86* (9), 4068−4077.
(3) Ishibashi, R.; Mawatari, K.; Kitamori, T. *Small* **2012**, *8* (8), 1237−1242.
(4) Pennathur, S.; Baldessari, F.; Santiago, J. G.; Kattah, M. G.; Steinman, J. B.; Utz, P. J. *Anal. Chem.* **2007**, *79* (21), 8316−8322.
(5) Kato, M.; Inaba, M.; Tsukahara, T.; Mawatari, K.; Hibara, A.; Kitamori, T. *Anal. Chem.* **2010**, *82* (2), 543−547.
(6) Duan, L.; Cao, Z.; Yobas, L. *Anal. Chem.* **2016**, *88* (23), 11601−11608.
(7) Shimizu, H.; Smirnova, A.; Mawatari, K.; Kitamori, T. *J. Chromatogr. A* **2017**, *1490*, 11−20.
(8) Bard, A. J.; Faulkner, L. R. *Electrochemical Methods: Fundamentals and Applications*; Wiley: New York, 2001.
(9) Rucki, R. *Talanta* **1980**, *27* (2), 147−156.
(10) Goto, M.; Koyanagi, Y.; Ishii, D. *J. Chromatogr. A* **1981**, *208* (2), 261−268.
(11) Mitton, K. P.; Trevithick, J. R. *Methods Enzymol.* **1994**, *233* (C), 523−539.
(12) Trojanowicz, M. *Anal. Chim. Acta* **2011**, *688* (1), 8−35.
(13) Hashemi, P.; Dankoski, E. C.; Petrovic, J.; Keithley, R. B.; Wightman, R. M. *Anal. Chem.* **2009**, *81* (22), 9462−9471.
(14) Heien, M. L. A. V; Phillips, P. E. M.; Stuber, G. D.; Seipel, A. T.; Wightman, R. M. *Analyst* **2003**, *128* (12), 1413−1419.
(15) Hermans, A.; Seipel, A. T.; Miller, C. E.; Wightman, R. M. *Langmuir* **2006**, *22* (5), 1964−1969.
(16) Wilson, G. S.; Johnson, M. A. *Chem. Rev.* **2008**, *108* (7), 2462−2481.
(17) Wang, J.; Ariel, M. *J. Electroanal. Chem. Interfacial Electrochem.* **1977**, *83* (2), 217−224.
(18) Unwin, P. R.; Compton, R. G. Chapter 6 The Use of Channel Electrodes in the Investigation of Interfacial Reaction Mechanisms. In *Comprehensive Chemical Kinetics*; Elsevier: New York, 1989; Vol. *29*, pp 173−296.
(19) Wang, J. *Comprehensive Analytical Chemistry* **2007**, *49*, 131−141.
(20) Florence, T. M. *J. Electroanal. Chem. Interfacial Electrochem.* **1984**, *168* (1−2), 207−218.
(21) Johnson, D. C.; Polta, J. A.; Polta, T. Z.; Neuburger, G. G.; Johnson, J.; Tang, A. P.-C.; Yeo, I.-H.; Baur, J. *J. Chem. Soc., Faraday Trans. 1* **1986**, *82* (4), 1081.
(22) Kalvoda, R.; Kopanica, M. *Pure Appl. Chem.* **1989**, *61* (1), 97−112.
(23) Heien, M. L. a V; Johnson, M. a; Wightman, R. M. *Anal. Chem.* **2004**, *76* (19), 5697−5704.
(24) Bucher, E. S.; Wightman, R. M. *Annu. Rev. Anal. Chem.* **2015**, *8*, 239−261.
(25) Song, Y.; Heien, M. L. A. V.; Jimenez, V.; Wightman, R. M.; Murray, R. W. *Anal. Chem.* **2004**, *76* (17), 4911−4919.
(26) Bath, B. D.; Michael, D. J.; Trafton, B. J.; Joseph, J. D.; Runnels, P. L.; Wightman, R. M. *Anal. Chem.* **2000**, *72* (24), 5994−6002.
(27) Ross, A. E.; Venton, B. J. *Anal. Chem.* **2014**, *86* (15), 7486−7493.
(28) Dengler, A. K.; McCarty, G. S. *J. Electroanal. Chem.* **2013**, *693*, 28−33.
(29) Atcherley, C. W.; Laude, N. D.; Parent, K. L.; Heien, M. L. *Langmuir* **2013**, *29* (48), 14885−14892.
(30) Robinson, D. L.; Venton, B. J.; Heien, M. L. a V; Wightman, R. M. *Clin. Chem.* **2003**, *49* (10), 1763−1773.
(31) Fonash, S. J.; Liang, H.; Nam, W. J. A Novel Parallel Flow Control (PFC) System for Syringe-Driven Nanofluidics. In *Nanotechnology 2008: Microsystems, Photonics, Sensors, Fluidics, Modeling, and Simulation − Technical Proceedings of the 2008 NSTI Nanotechnology Conference and Trade Show*; CRC Press, Boca Raton, FL, 2008; Vol. 3, p 281−283.
(32) Mathwig, K.; Lemay, S. G. *Electrochim. Acta* **2013**, *112*, 943−949.
(33) Mathwig, K.; Mampallil, D.; Kang, S.; Lemay, S. G. *Phys. Rev. Lett.* **2012**, *109* (11), 118302.
(34) Wopschall, R. H.; Shain, I. *Anal. Chem.* **1967**, *39* (13), 1514−1527.
(35) Kang, S.; Mathwig, K.; Lemay, S. G. *Lab Chip* **2012**, *12* (7), 1262.
(36) Cuharuc, A. S.; Zhang, G.; Unwin, P. R. *Phys. Chem. Chem. Phys.* **2016**, *18* (6), 4966−4977.
(37) Tan, S. Y.; Zhang, J.; Bond, A. M.; Macpherson, J. V.; Unwin, P. R. *Anal. Chem.* **2016**, *88* (6), 3272−3280.
(38) Hlushkou, D.; Gritti, F.; Guiochon, G.; Seidel-Morgenstern, A.; Tallarek, U. *Anal. Chem.* **2014**, *86* (9), 4463−4470.
(39) Hlushkou, D.; Gritti, F.; Daneyko, A.; Guiochon, G.; Tallarek, U. *J. Phys. Chem. C* **2013**, *117* (44), 22974−22985.
(40) Deinhammer, R. S.; Ting, E.-Y.; Porter, M. D. *J. Electroanal. Chem.* **1993**, *362* (1−2), 295−299.

DOI: 10.1021/acs.analchem.8b01719
Anal. Chem. 2018, 90, 7127−7130